Upper Bound Analysis of Cyclic Expansion Extrusion

M. M. Samandari, S.H.R. Torabi, Ghader Faraji *

School of Mechanical Engineering, College of Engineering, University of Tehran, Tehran, 11155-4563, Iran

ARTICLE INFO

Article history:

Received 13 September 2016
Accepted 4 April 2017
Available online 25 June 2017

Keywords:

Severe plastic deformation
Cyclic expansion extrusion
Upper bound analysis
Finite element method

ABSTRACT

Deformation of the material during cyclic expansion extrusion (CEE) is investigated using upper-bound theorem. The analytical approximation of forming loads agrees very well with the FEM results for different amounts of chamber diameter, friction factor and also for lower die angles. However, the difference between analytical and numerical solution increases at higher die angles, which is explained by the formation of dead-metal zones at these angles. The results show that the forming load increases at higher friction coefficients, higher chamber diameters, and lower amounts of corner fillet radius, but for the die angle there is a maximum value of load at about 60°. Forming load is enhanced by the increase of the die chamber diameter and friction factor. Increasing the die chamber diameter causes higher strains and, therefore, higher rate of homogenous work. The load slightly decreased by an increase of the die corner radius because of the lower and more homogeneous strain distribution in the material.

1-Introduction

Severe plastic deformation (SPD) processes are defined as material forming methods to create ultra-fine grained (UFG) and nanostructured metals via application of ultra-large plastic strains [1-3]. Due to the superior and unique mechanical properties of the UFG materials fabricated by SPD, various techniques such as equal channel angular pressing/extrusion (ECAP/ECAE) [4-7], accumulative roll bonding (ARB) [8, 9], high pressure torsion (HPT) [10, 11], cyclic extrusion compression (CEC) [12, 13], and many other processes were developed [14-16]. Recently, a method was proposed by Pardis et al. [17] as a modified counterpart of cyclic extrusion-compression (CEC) entitled as cyclic expansion extrusion (CEE). In this process, the extrusion part of the process is carried out after the material experiences expansion. Although there are some reported works focusing on strain distribution in CEC [18, 19] and mechanical aspects of the process by means of the finite element method (FEM) [20], the CEE process has not been studied in detail. In the previous article by the authors, FEM simulations are used to investigate the effects of the parameters on strain distribution of samples during CEE process on circular cross sections [21].

On the other hand, evaluation of the mechanics of deformation and prediction of the forming loads help engineers to come up with a better design of the tools as well as better prediction of the results of the processes [22]. Deformation of materials and prediction of the forming loads in metal forming methods especially SPD have been studied by many researchers with numerical and analytical methods. Most of the analytical investigations were focused on the ECAP [23, 24], ECAE [25, 26] and tubular

* Corresponding author:
E-mail address: ghfaraji@ut.ac.ir

channel angular pressing (TCAP) [27, 28], but there is no work on predicting the forming load of the CEE process using theoretical investigations. In this article, the required forming load for the CEE method was investigated using the analytical upper bound method and the predicted force was then compared to the numerical FE method.

Schematic illustrations of the CEE process and the die parameters are shown in Fig. 1. The method is a cyclic process in which the cross section of the material will increase to the chamber diameter (D_3) and will subsequently decrease using the extrusion half cycle of the process to the initial diameter (D_1). The material experiences two half cycles of deformation including expansion and extrusion stages. So, it is obvious that one advantage of the CEE process compared to CEC is that the force required to extrude the metal provides a proper amount of back-pressure for the expansion and, therefore, no additional back-pressure is needed. Moreover, the forming loads are lower in comparison with the CEC method [17].

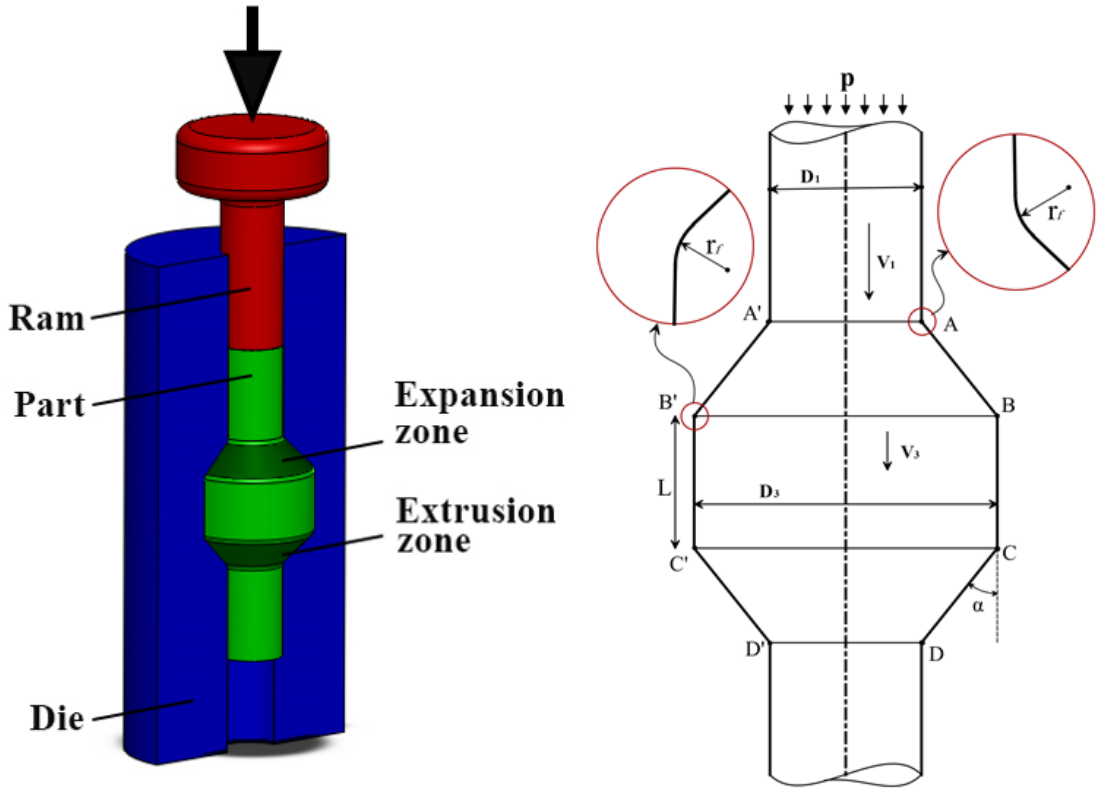

Fig. 1. Schematic illustrations of the CEE process and die parameters.

2- Upper-Bound Analysis

The upper-bound method is used to calculate the external force by equating the rate of external work with the rate of internal energy consumption, which can be written as [29]:

$$\dot{W}_a = \dot{W}_s + \dot{W}_h + \dot{W}_f \quad (1)$$

where $\dot{W}_a$ is the rate of external work, $\dot{W}_s$ is the total energy dissipation along the shear discontinuities, $\dot{W}_h$ is the rate of homogeneous work, and $\dot{W}_f$ represents the rate of frictional work. In this approach, a simplifying assumption is made according to which there is no strain hardening for the material.

Fig. 2 schematically shows the material in a die of angle α with a constant interface shear stress mk, where m refers to the friction factor and k is the yield strength in shear. In region 1, the material moves toward the expansion zone as a rigid body (rigid body motion) with a constant velocity (V_1). The deformation zone separates

region 2 from regions 1 and 3 by entry and exit disk surfaces of *AA'* and *BB'* which are the beginning and the ending surfaces of the first deformation zone, respectively (Fig. 2 (a)). In the first deformation zone (region 2), the material is expanded and undertakes plastic strains. Region 3 is where no further deformation takes place and the material moves to the second half cycle of the process with a constant velocity of V_3. It must be noted that volume constancy of the material results in

$$V_3 = (R_1/R_3)^2 V_1 = (R_1/R_3)^2 V_5 \quad (2)$$

where R_i and V_i are the die cavity radios and material velocity in the *i*th region, respectively. All material paths are horizontal before crossing the *AA'* disk and after crossing the *BB'* disk in the first half cycle. All of the elements on a specific cross-sectional disk between *AA'* and *BB'* have the same horizontal component of velocity, V_x, but V_x decreases for different disks from *AA'* to *BB'*.

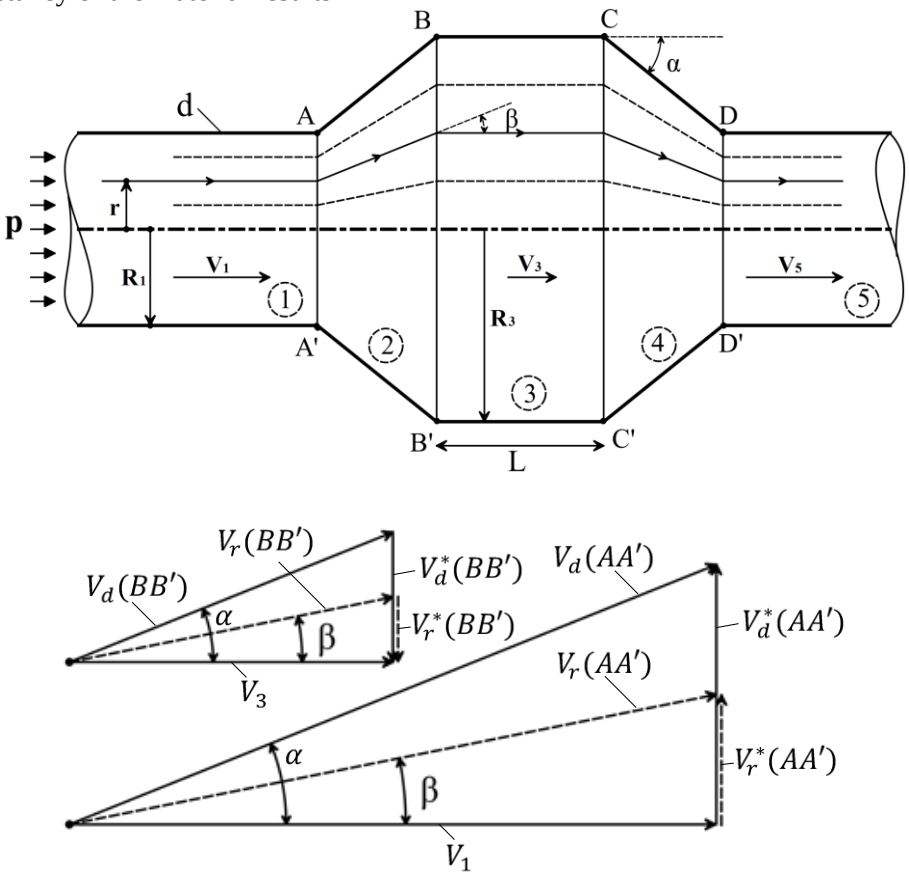

Fig. 2. (a) Material flow and deformation regions, and (b) hodograph of velocities during deformation.

2-1- Energy dissipation along the shear discontinuity, $\dot{W}_s$

When a particle crosses *AA'* it bears a velocity discontinuity, $V^*(AA')$, which depends on the radial distance *r* from the centerline. As can be seen from the hodograph of Fig. 2 (b), at the outer surface *d*, $V_d^*(AA') = V_1 \tan \alpha$, and at the centerline, $V^*(AA') = 0$. At other points we have:

$$V_r^*(AA') = V_1 (r / R_1) \tan \alpha \quad (3)$$

Using this equation, the rate of shear work along *AA'* discontinuity is [29]:

$$\dot{W}_s(AA') = \int_0^{R_1} 2\pi r\, k\, V_1 \left(\frac{r}{R_1}\right) \tan\alpha \, dr$$

$$= (2/3)\pi R_1^2 k V_1 \tan\alpha \quad (4.1)$$

In like manner for *BB'* discontinuity and substituting $V_3 = (R_1/R_3)^2 V_1$ from equation (2)[29] we have:

$$\dot{W}_s(BB') = \int_0^{R_3} 2\pi r\, k\, V_3 \left(\frac{r}{R_3}\right) \tan\alpha\, dr$$
$$= (2/3)\pi R_1^2 k V_1 \tan\alpha \qquad (4.2)$$

Likewise, in the second half cycle, extrusion, we have:

$$\dot{W}_s(CC') = \dot{W}_s(BB') \qquad (4.3)$$
$$\dot{W}_s(DD') = \dot{W}_s(AA') \qquad (4.4)$$

Substituting equations (4.1) to (4.4), the total energy dissipation along the shear discontinuities is:

$$\dot{W}_s = (8/3)\pi R_1^2 k V_1 \tan\alpha \qquad (4.5)$$

2-2- Rate of homogeneous work

Specific homogeneous work, w_h could be calculated from stress strain curves. In the rigid-perfectly plastic model, it is simplified as:

$$w_h = \sigma_y \bar{\varepsilon} \qquad (5)$$

Where σ_y represents the yield strength of the material and $\bar{\varepsilon}$ is the total equivalent strain in the process. The total equivalent strain in a half cycle of the CEE process can be calculated as [21]:

$$\bar{\varepsilon} = 2\ln(R_3/R_1) \qquad (6)$$

Therefore, the homogeneous work rate for the first half cycle (i.e. deformation in region 2) is:

$$\dot{W}_h(reg.2) = w_h\, V_1 \pi R_1^2 = \sigma_y \bar{\varepsilon}\, V_1 \pi R_1^2 \qquad (7)$$

Substituting $\bar{\varepsilon}$ from equation (6), using Tresca Criterion and accounting 2 half cycles, we have:

$$\dot{W}_h = 8k \ln(R_3/R_1) V_1 \pi R_1^2 \qquad (8)$$

2-3- Rate of frictional work

Like equation (2), for a slab of radius R_2 in the region 2, the horizontal component of velocity is:

$$V_x = V_1 (R_1/R_2)^2 \qquad (9)$$

So, the sliding velocity at the interface, V_s, is:

$$V_s = V_1 (R_1/R_2)^2 / \cos\alpha \qquad (10)$$

The area of the element in contact with the die is then $2\pi R_2\, dR_2/\sin\alpha$. Thus, by using equation (10) [29]:

$$\dot{W}_f(reg.2) = \left| \int_{R_1}^{R_3} \frac{V_1 R_1^2}{R_2^2 \cos\alpha} \frac{2\pi R_2}{\sin\alpha} mk\, dR_2 \right|$$
$$= 4\pi m k V_1 R_1^2 \ln\frac{R_3}{R_1} / \sin 2\alpha \qquad (11.1)$$

Likewise, in region 4, extrusion, we have:

$$\dot{W}_f(reg.4) = \dot{W}_f(reg.2) \qquad (11.2)$$

Moreover, for region 3:

$$\dot{W}_f(reg.3) = 2\pi R_3 L\, V_3 mk \qquad (11.3)$$

Substituting equations (11.1) to (11.3) and using equation (2), the rate of total frictional work is:

$$\dot{W}_f = 2\pi m k V_1 R_1^2 \left(\frac{4\ln\frac{R_3}{R_1}}{\sin 2\alpha} + \frac{L}{R_3} \right) \qquad (12)$$

2-4- External Force

The external wok rate can be calculated as:

$$\dot{W}_a = pV_1 \pi R_1^2 \qquad (13)$$

By substituting equations (5), (8), (12) and (13) and simplifying, the upper-bound external pressure will be:

$$p = (8/3)k \tan\alpha + 8k \ln(R_3/R_1) + 2mk(4\ln\frac{R_3}{R_1}/\sin 2\alpha + L/R_3) \qquad (14)$$

Finally, knowing that the force is a multiplication of the pressure by the acting area, we have:

$$F = F_d + F_h + F_f = p\pi R_1^2 \qquad (15)$$

where F_d, F_h and F_f stand for the forces that correspond to velocity discontinuities, homogenous work and frictional work, respectively.

3- The FEM procedure

Simulations were done using the commercial DEFORM-3D software. An automatic remeshing was employed in the simulations to accommodate the imposed large strains for more accuracy of the results. It is necessary to properly define the material behavior, boundary conditions and FEM parameters like elements and solving method. 1/16 of the work-piece and dies was simulated in the FEM because of the symmetric nature of the process. Die angle (α), chamber diameter (D_3), and corner fillet radius (r_f) were considered as variable die parameters as shown in Fig. 1. Also, the friction factor (m) was considered as a variable parameter for the investigation of the forming loads in the CEE process. The die parameters and their values employed in the simulations are listed in Table 1. The initial diameter of the cylindrical sample (D_1) and the length of the chamber (L) are equal to 10 mm. FEM parameters used for simulations are given in Table 2. The material properties of the pure aluminum employed in FEM analysis is also described in Table 2 and corresponds to a Hollomon-type material behavior, with $\sigma = K\varepsilon^n$ [30]. Also, the rigid perfectly plastic model is used for the analytical method. The stress-strain curve of the material used for simulations and an analytical model is shown in Fig. 3.

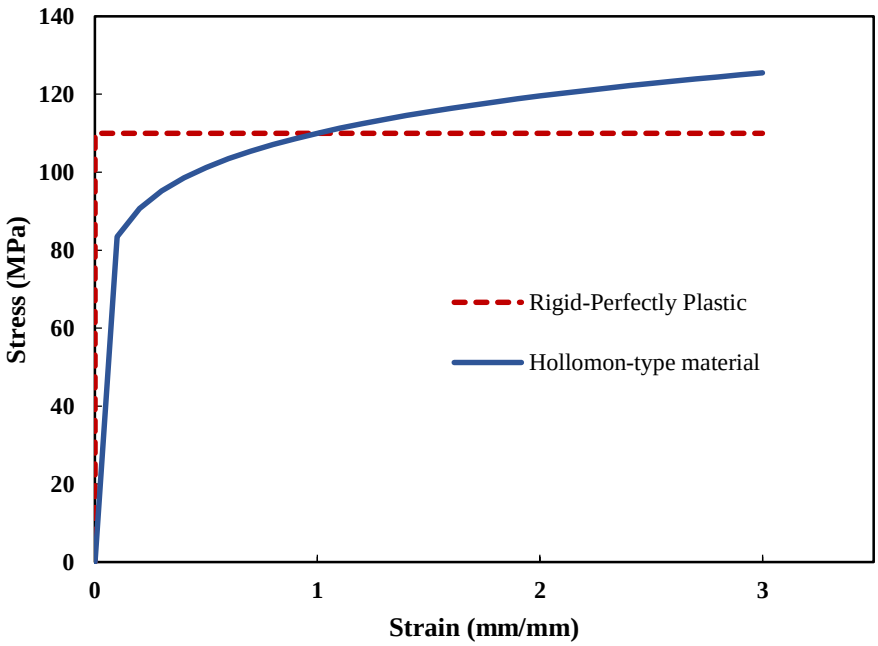

Fig. 3. The material behavior of pure aluminum at room temperature for FEM and the corresponding rigid-perfectly plastic model for the analytical solution.

Table 1. Variable parameters and simulation condition.

Variable parameter	Levels	Other parameters			
		α (°)	**D_3 (mm)**	**m**	**r (mm)**
Die angle, α (°)	30, 45, 60, 75, 90	-	20	0.1	1
Chamber diameter (D_3)	15, 20, 25	45	-	0.1	1
Friction factor (m)	0, 0.1, 0.2, 0.3	45	20	-	1
Corner fillet radius (r)	0.5, 1, 1.5, 2	45	20	0.1	-

Table 2. FE parameters used for the simulations.

Parameter	Value	
	Die	**Workpiece**
Material	Rigid	**Pure aluminum**
Strength Coefficient (MPa)	-	**110**
Strain hardening exponent	-	**0.12**
Yield strength (MPa)	-	**80**
Density (g/cm^3)	-	**2.71**
Poisson's ratio	-	**0.33**
Temperature (ºC)	20	**20**
Type of elements	**tetrahedral**	
Ram Speed, V_1 (mm/s)	**1**	

4- Results and Discussion

Based on the analytical model, velocity discontinuities on the entry and exit surfaces, *AA', BB', CC' and DD'*, causes shear strains and stresses along the boundary surfaces. These velocity discontinuities and the resulted shear stresses are the main causes of the grain fragmentation. By exceeding these shear stresses from the shear strength of the material, the grains start fragmentation and, consequently, the grain refinement process takes place. The proposed analytical model is compared to the FEM results for the first pass of CEE. The parameters of FEM simulation are shown in Table 1. For evaluating the FEM results and comparing with an analytical approach, the average value from a steady region of forming load diagram is obtained, as illustrated in Fig. 4.

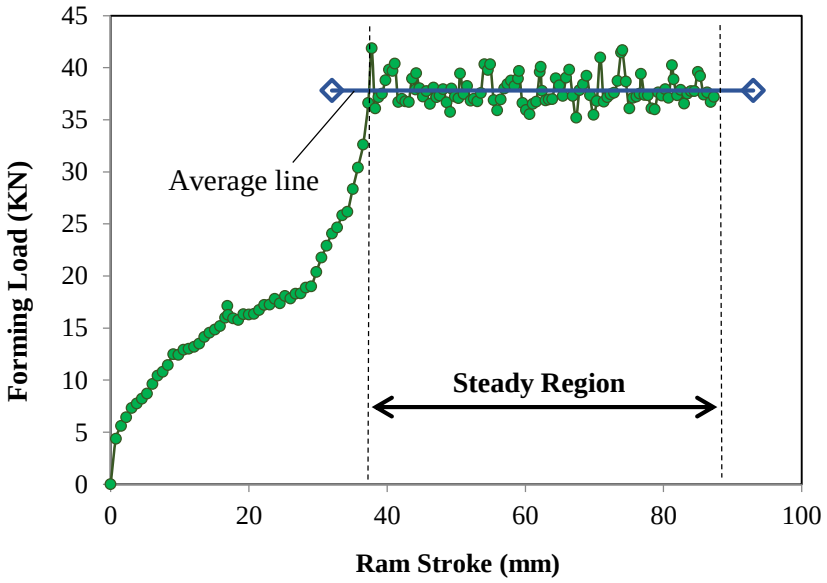

Fig. 4. Forming load diagram during the first pass of CEE obtained from FE Simulation; average value is used for evaluating FEM results. α=60º, D_3=20mm, r_f=1mm and m=0.1.

4-1- Effect of the die Angle

The effect of the die angle on the forming load has been investigated using analytical and FEM approaches for α=30˚, 45˚, 60˚, 75˚ and 90˚. As can be observed in Fig. 5, in lower angles, the upper-bound results are in good agreement with numerical simulation. However, the analytical values have an increasing trend, while the forming load in the FEM results increases up to α=60° and then decreases and the curve has a quadratic parabolic model. This is due to the forming of dead metal zone shown in the

contours of Fig. 5 which cannot be considered in the upper bond analysis. These contours show the velocity of the material flow in the die: the material velocity of yellow areas is more than 0.01 mm/s and for black areas it is less than 0.01 mm/s. So, it can be concluded that increasing the die angle leads to an increase in the area of the dead metal zones in the cornesrs. These dead zones prevent the material to completely enter the die chamber and therefore a virtual chamber with lower die angle. The material velocity for all simulated die angles is shown in Fig. 6. As it is distinct for 30° and 45° angles, the velocity of material flow is uniform, while the uniformity decreases with increasing the die angle. Therefore, the material almost passes without experiencing complete velocity discontinuities at 75° and 90° die angles as discussed earlier. On the other hand, the proposed upper bound analysis does not consider the effect of the dead metal zone resulted from the higher velocity discontinuities and higher sliding velocity of the material at higher die angles. So, the forming load in the upper bound analysis increases with increasing the die angle (Eq. (5)).

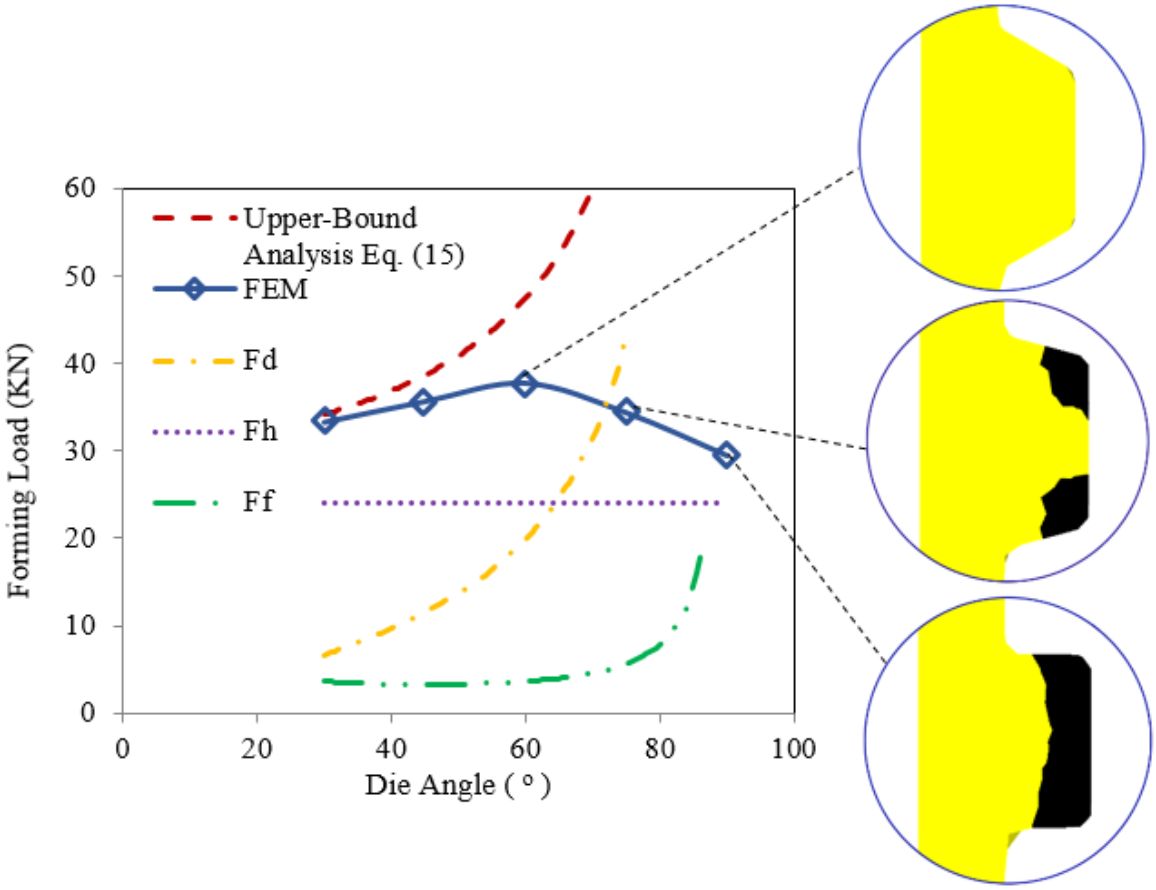

Fig. 5. Effect of the die angle, α, on the forming load.

4-2- Effect of chamber diameter

The effect of die chamber diameter on the forming load was investigated for D_3=15mm, 20mm and 25 mm. Variation of the forming load is shown in Fig. 7 for both FEM and upper bound analysis. This figure shows that the forming load enhances with increasing the chamber diameter. At higher chamber diameters, the rate of homogeneous work is greater than at the lower ones and this factor causes higher forming loads (Eq. (8)). This is because of the higher strains at higher chamber diameters (Fig. 8). Therefore, at higher diameters of the die chamber, the material flow occurs with more difficulty in comparison with the lower diameters.

Also, the curve of the forming load variation obtained from the upper bound analysis is shown

in Fig. 7. As can be seen, the analysis provides values that are a little greater than the FEM results. It is because the upper bound analysis over-estimates the actual loads needed for the process, but the predicted values will be close to the actual ones if the method is used properly [22]. As it is shown, the error of the analysis is lower than 10% which is a good acquisition.

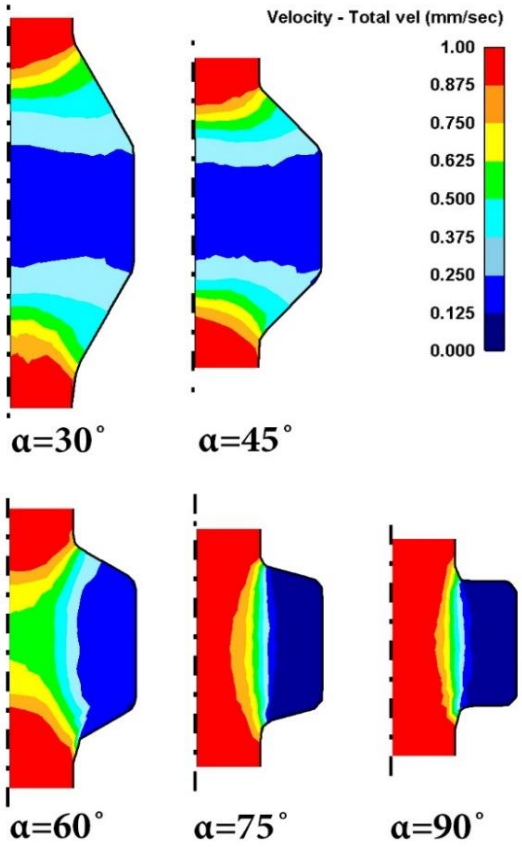

Fig. 6. Velocity of the material in the die chamber for different angles, α=30˚ up to 90˚.

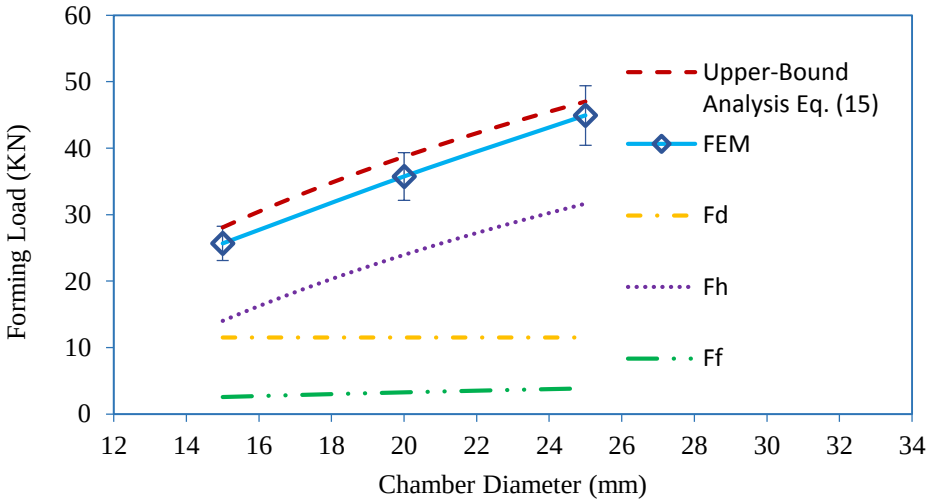

Fig. 7. The effect chamber diameter on the forming load.

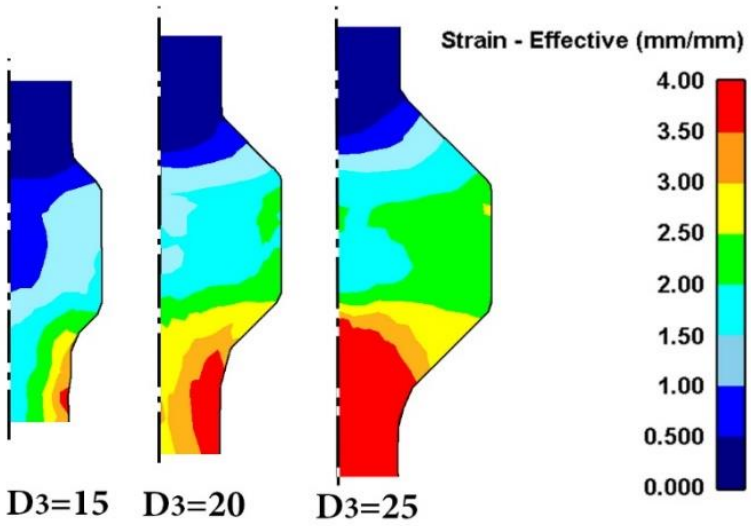

Fig. 8. The strain distribution for different chamber diameters, D_3=15 mm, 20 mm and 25 mm.

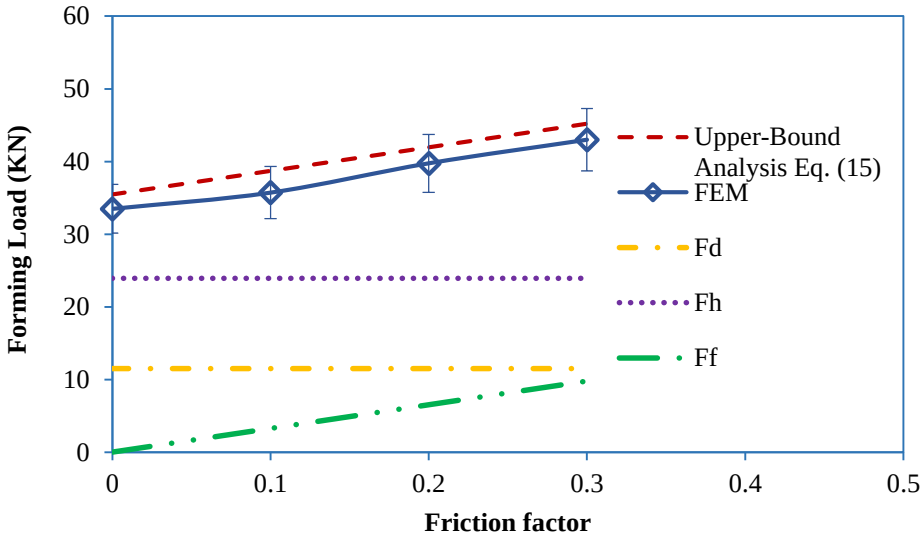

Fig. 9. The effect of friction factor on the forming load.

4-3- Effect of friction factor

To investigate the effect of friction factor on the forming load, the values of the load were obtained from the software for different friction factors of *m*=0, 0.1, 0.2 and 0.3. Fig. 9 shows the effect of the friction factor on the forming load resulted from analytical and FEM approaches. As can be seen, the effect of the frictional work is less than homogenous work and energy dissipation for velocity discontinuities. But in higher friction factors, it can reach other forces. Fig. 10 shows that at higher friction factors, the material flow occurs with more difficulty. Also, according to the FEM results, it can be seen that the forming load increases by enhancing the friction factor. As discussed earlier, because of the over-estimation, the upper-bound values are greater that the FEM ones. However, the values are inside the error bars and, therefore, it can be concluded that the error of the analysis is lower than 10%.

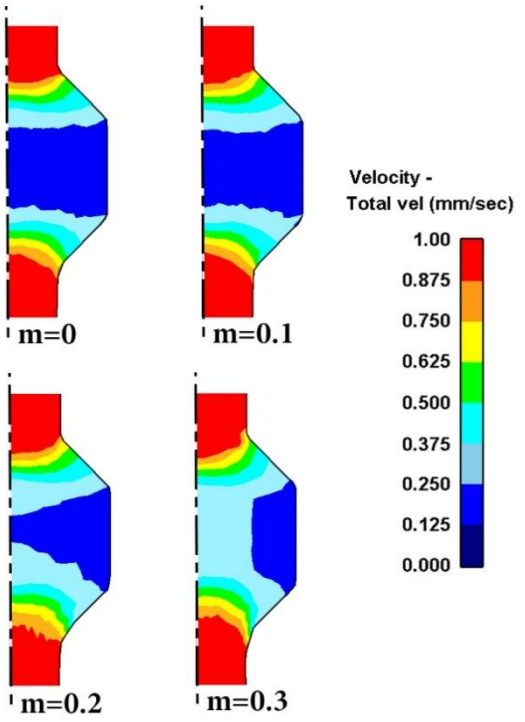

Fig. 10. The velocity of material at the die chamber for different friction factors of m=0 to 0.3.

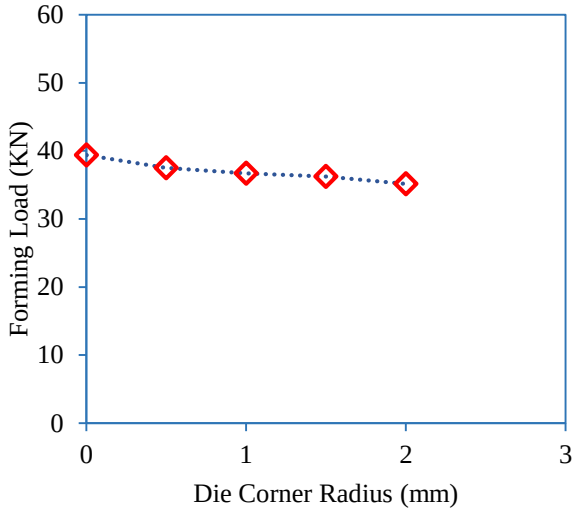

Fig. 11. The effect of the die corner radius on the forming load resulted from FEM.

4-4- Effect of die corner radius

Fig. 11 shows variation of the forming load at various levels of the corner radius, r_f= 0, 0.5, 1, 1.5 and 2 mm. As can be seen, the forming load decreases with increasing the corner radius due to more fluency in the material flow. Fig. 12 shows the effect of die corner radius on the strain within the material. As can be observed, smaller corner radius causes higher strains and also nonhomogeneous strain distribution [21]. Therefore, the process requiresmore external forces to take place. The effect of the corner radius is not considered in the upper-bound analysis; thus, only the FEM results are shown.

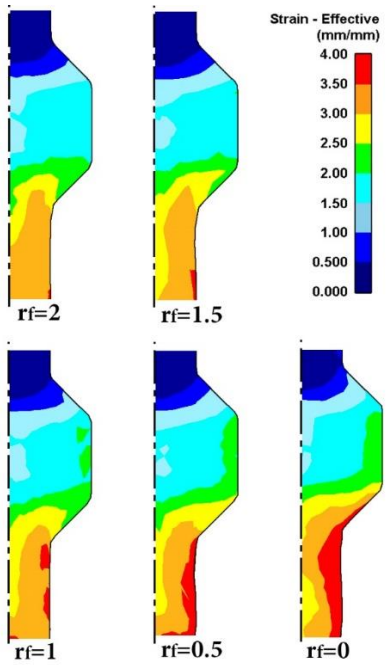

Fig. 12. The Strain distribution in die for different die corner radii, r_f = 0, 0.5, 1, 1.5 and 2 mm.

5- Conclusions

In this study, upper bound analysis was carried out to predict the forming load of the CEE process. Also, the effects of die and process parameters on the forming load were evaluated using FEM. Then the results of analytical approach and FEM were compared, and these results showed excellent correspondence with negligible error in lower die angles. For high values of the die angle, the upper bound failed to predict the forming loads because of the effect of dead metal zones. In addition, the following conclusions were achieved:

- The die angle had a parabolic shape effect on the forming load so that the forming load increased with increasing the angle and then the load decreased after the angle of 60°. It is because of the effect of dead metal zone that rises at high angles.

- The forming load was enhanced with increasing the die chamber diameter and the friction factor. Increasing the die chamber diameter causes higher strains and, therefore, higher rate of homogenous work.
- The forming load slightly decreased with an increase of die corner radius because of the lower and more homogeneous strain distribution in the material.

Acknowledgement

This work was supported by Iranian National Science Foundation (INSF).

References

[1] Rosochowski, A. *Processing metals by severe plastic deformation*. in *Solid State Phenomena*. 2004. Trans Tech Publ.

[2] Rosochowski, A., L. Olejnik, and M. Richert, *Metal forming technology for producing bulk nanostructured metals.* Journal of Steel and Related Materials–Steel GRIPS, 2004. 2: pp. 35-44.

[3] Valiev, R.Z., et al., *Producing bulk ultrafine-grained materials by severe plastic deformation.* Jom, 2006. 58(4): pp. 33-39.

[4] Altan, B., G. Purcek, and I. Miskioglu, *An upper-bound analysis for equal-channel angular extrusion.* Journal of materials processing technology, 2005. 168(1): pp. 137-146.

[5] Valiev, R.Z. and T.G. Langdon, *Principles of equal-channel angular pressing as a processing tool for grain refinement.* Progress in Materials Science, 2006. 51(7): pp. 881-981.

[6] Azushima, A., et al., *Severe plastic deformation (SPD) processes for metals.* CIRP Annals-Manufacturing Technology, 2008. 57(2): pp. 716-735.

[7] Azimi, A., et al., *Mechanical properties and microstructural evolution during multi-pass ECAR of Al 1100–O alloy.* Materials & Design, 2012. 42: pp. 388-394.

[8] Saito, Y., et al., *Ultra-fine grained bulk aluminum produced by accumulative roll-bonding (ARB) process.* Scripta materialia, 1998. 39(9): pp. 1221-1227.

[9] Huang, X., et al., *Microstructural evolution during accumulative roll-bonding of commercial purity aluminum.* Materials Science and Engineering: A, 2003. 340(1): pp. 265-271.

[10] Zhilyaev, A., et al., *Experimental parameters influencing grain refinement and microstructural evolution during high-pressure torsion.* Acta Materialia, 2003. 51(3): pp. 753-765.

[11] Zhilyaev, A.P. and T.G. Langdon, *Using high-pressure torsion for metal processing: Fundamentals and applications.* Progress in Materials Science, 2008. 53(6): pp. 893-979.

[12] Richert, M., Q. Liu, and N. Hansen, *Microstructural evolution over a large strain range in aluminium deformed by cyclic-extrusion–compression.* Materials Science and Engineering: A, 1999. 260(1): pp. 275-283.

[13] Zhang, J. *A new bulk deformation method–Cyclic extrusion*. in *Materials Science Forum*. 2007. Trans Tech Publ.

[14] Faraji, G., et al., *Parallel tubular channel angular pressing (PTCAP) as a new severe plastic deformation method for cylindrical tubes.* Materials Letters, 2012. 77: pp. 82-85.

[15] Babaei, A., et al., *Repetitive forging (RF) using inclined punches as a new bulk severe plastic deformation method.* Materials Science and Engineering: A, 2012. 558: pp. 150-157.

[16] Faraji, G., M.M. Mashhadi, and H.S. Kim, *Tubular channel angular pressing (TCAP) as a novel severe plastic deformation method for cylindrical tubes.* Materials Letters, 2011. 65(19): pp. 3009-3012.

[17] Pardis, N., et al., *Cyclic expansion-extrusion (CEE): A modified counterpart of cyclic extrusion-compression (CEC).* Materials Science and Engineering: A, 2011. 528(25): pp. 7537-7540.

[18] Lin, J., et al., *Study on deformation behavior and strain homogeneity during cyclic extrusion and compression.* Journal of materials science, 2008. 43(21): pp. 6920-6924.

[19] LIN, J.-b., et al., *Finite element analysis of strain distribution in ZK60 Mg alloy during cyclic extrusion and compression.* Transactions of Nonferrous Metals Society of China, 2012. 22(8): pp. 1902-1906.

[20] Rosochowski, A., R. Rodiet, and P. Lipinski, *Finite element simulation of cyclic extrusion-compression.* Metal forming, 2000: pp. 253-259.

[21] TORABI, H., et al., *Numerical investigation of strain distribution during cyclic*

expansion extrusion (CEE). Journal of Advanced Materials and Processing, 2015. 3(2): pp. 35-48.
[22] Talebanpour, B. and R. Ebrahimi, *Upper-bound analysis of dual equal channel lateral extrusion.* Materials & Design, 2009. 30(5): pp. 1484-1489.
[23] Medeiros, N. and L. Moreira, *Upper-bound analysis of die corner gap formation for strain-hardening materials in ECAP process.* Computational Materials Science, 2014. 91: pp. 350-358.
[24] Alkorta, J. and J.G. Sevillano, *A comparison of FEM and upper-bound type analysis of equal-channel angular pressing (ECAP).* Journal of Materials Processing Technology, 2003. 141(3): pp. 313-318.
[25] Reihanian, M., R. Ebrahimi, and M. Moshksar, *Upper-bound analysis of equal channel angular extrusion using linear and rotational velocity fields.* Materials & Design, 2009. 30(1): pp. 28-34.
[26] Paydar, M., et al., *An upper-bound approach for equal channel angular extrusion with circular cross-section.* Journal of materials processing technology, 2008. 198(1): pp. 48-53.
[27] Faraji, G., et al., *An upper-bound analysis for frictionless TCAP process.* Archive of Applied Mechanics, 2013. 83(4): pp. 483-493.
[28] Faraji, G., et al., *Deformation behavior in the tubular channel angular pressing (TCAP) as a noble SPD method for cylindrical tubes.* Applied Physics A, 2012. 107(4): pp. 819-827.
[29] Hosford, W.F. and R.M. Caddell, *Metal forming: mechanics and metallurgy*. 2011: Cambridge University Press.
[30] Sevillano, J.G., P. Van Houtte, and E. Aernoudt, *Large strain work hardening and textures.* Progress in Materials Science, 1980. 25(2): pp. 69-134.